

Shear behavior of hollow clay brick masonry wallet coated with short jute fiber reinforced mortar

 L.N. Farias^a,  P.R.L. Lima^{a,b},  R.D. Toledo Filho^a

a. Federal University of Rio de Janeiro (Rio de Janeiro, Brasil)

b. State University of Feira de Santana (Bahia, Brasil)

 lidianne.farias@coc.ufrj.br

Received 26 January 2024

Accepted 27 April 2024

Available on line 23 May 2024

ABSTRACT: The objective of this study is to present a new method of reinforcing masonry using layers of mortar reinforced with short jute fibers. Mortars were produced with 0%, 2% and 3% jute fibers with cementitious matrices free of calcium hydroxide. The effectiveness of the reinforced mortar was evaluated through diagonal compression tests of hollow ceramic brick masonry prisms. The prisms were coated on both sides. The experimental results demonstrated that the diagonal resistance of the fiber system increased by 28 to 30% and presented greater resistance to elastic deformation during load application, with deformation coefficients 2 and 3 times greater for 2% and 3% of fibers, respectively. Therefore, jute fibers prove to be a sustainable and efficient alternative for masonry reinforcement applications, with maximum applied loads considerably higher than the unreinforced system, in addition to better crack control.

KEY WORDS: Natural fiber; Shear stress; Diagonal compression; Hollow bricks.

Citation/Citar como: Farias LN, Lima PRL, Toledo Filho RD. 2024. Shear behavior of hollow clay brick masonry wallet coated with short jute fiber reinforced mortar. Mater. Construcc. 74(354):e347. <https://doi.org/10.3989/mc.2024.374624>.

RESUMEN: *Comportamiento al corte de la mampostería de ladrillos huecos de arcilla recubiertos con mortero reforzado con fibras cortas de yute.* El objetivo de este estudio es presentar un nuevo método de refuerzo de mampostería mediante capas de mortero reforzado con fibras cortas de yute. Se produjeron morteros con 0%, 2% y 3% de fibras de yute con matrices cementantes libres de hidróxido de calcio. La efectividad del mortero armado se evaluó mediante ensayos de compresión diagonal de prismas de mampostería de ladrillo cerámico hueco. Los prismas estaban recubiertos por ambas caras. Los resultados experimentales demostraron que la resistencia diagonal del sistema de fibras aumentó entre un 28 y un 30%, y presentó mayor resistencia a la deformación elástica durante la aplicación de carga, con coeficientes de deformación 2 y 3 veces mayores para el 2% y 3% de fibras, respectivamente. Por lo tanto, las fibras de yute demuestran ser una alternativa sostenible y eficiente para aplicaciones de refuerzo de mampostería, con cargas máximas aplicadas considerablemente mayores que el sistema no reforzado, además de un mejor control de fisuras.

PALABRAS CLAVE: Fibra natural; Esfuerzo cortante; Compresión diagonal; Ladrillos huecos.

Copyright: ©2024 CSIC. This is an open-access article distributed under the terms of the Creative Commons Attribution 4.0 International (CC BY 4.0) License.

1. INTRODUCTION

Clay hollow bricks are widely used in various construction applications due to their lower cost for housing, ease of implementation, and reduced labor requirements. Additionally, they are sustainable due to the lesser volume of material used per square meter of masonry (hollow blocks consist of over 60% of their unit being hollow), providing better thermal comfort for housing compared to solid brick masonry. This solution becomes even more relevant due to the increasing population in developing countries, resulting in a higher demand for faster and cost-effective constructions (1). However, walls made with hollow bricks typically have lower resistance compared to solid brick walls, especially under lateral loads such as wind action and seismic tremors, which tend to cause masonry failures due to bending and diagonal shear (2-4). As a result, retrofitting techniques are usually required to enhance or correct the load-bearing capacity of masonry after in-plane and out-of-plane seismic actions (2-5).

Various techniques have been employed in reinforcing ceramic brick masonry, such as bracing, crack stitching and grout injection (6-9); insertion of steel bars in bed joints (10), and steel-reinforced grout joint systems (11, 12). Systems involving the application of rendering mortar have also been widely used, incorporating reinforcement with metal or fiber-reinforced polymer mesh (13-16), or fabrics (17-20). The application of some of these techniques in clay hollow brick masonry has resulted in increased lateral force and displacement capacity without significant damage to the rendering until the peak load occurs (21), as well as increased compressive strength and shear resistance (22). Despite the mechanical efficiency of this type of reinforcement, the application of mortar reinforced with short steel fibers (23, 24) or engineered cementitious composite reinforced with polyethylene (PE) fibers (25) for the recovery or reinforcement of masonry has proven to be a promising technique due to its ease of application compared to traditional techniques that require more labor and execution time. Another retrofit technique for masonry that has yielded good results is the application of fiber-reinforced lime-based grouts, which, according to the authors (26), are feasible in the case of historic masonry restoration.

The use of dispersed short fibers in mortar allows for greater toughness of the material, expanding the use of masonry reinforced with this technique. In addition to steel fibers, mortars can be reinforced with short plant fibers, which have a lower energy cost in production and are derived from renewable sources, resulting in a more sustainable solution. For this reason, plant fabrics have also been used as a retrofit system in masonry (20, 27, 28). Plant fibers exhibit excellent tensile strength (29, 30), appropriate adhesion with cementitious matrices (31), and their use as

mortar reinforcement increases the tensile strength of mortars, toughness, and crack control (32-40).

The application of plant fibers in cement-based materials has historically been met with skepticism due to potential durability issues associated with chemical incompatibility between cement hydration products and plant fibers. However, using mineral additives as a substitute for cement results in a matrix free of calcium hydroxide, providing greater durability to the composites (41). Additionally, due to their high-water absorption, plant fibers may experience dimensional variation when the mortar coating is subjected to normal wetting and drying cycles during use. As a result, there can be damage at the interface and a loss of fiber-matrix adhesion, impairing the mechanical performance of the coating. To prevent such damage, physical and chemical treatments (34, 42) have been successfully applied to plant fibers, reducing their water absorption and improving the interface with the cementitious matrix.

The objective of this study is to introduce a novel method for reinforcing masonry using layers of mortar reinforced with short jute fibers. This type of application represents a scientific and technological innovation, as cementitious composites with short vegetable fibers are not commonly employed for this purpose. The proposed study not only presents the properties of composites produced with short jute fibers but also evaluates how these fibers can modify the mechanical behavior, mode of failure, and modulus of deformation of the reinforced walls. Additionally, the proposed reinforcement method represents a new alternative for masonry reinforcement, offering greater applicability and faster execution than the retrofit method using fabric application.

To achieve this goal, the jute fibers were chemically treated to enhance their durability and adhesion, and were evaluated using scanning electron microscopy, X-ray diffraction, direct tension, and water absorption tests. Mortars reinforced with 2% and 3% jute fibers were produced with cementitious matrices free of calcium hydroxide and subjected to water absorption, compressive strength, and flexural strength tests. The efficacy of fiber-reinforced mortar as a masonry reinforcement element was then assessed through diagonal compression testing of prisms coated on both sides.

2. MATERIALS AND METHODS

2.1. Jute Fiber

2.1.1. Processing and treatment

Jute fibers are produced in various regions worldwide, such as Bangladesh, China, India, Thailand, and Brazil, and are widely used in various textile ap-

plications, making them attractive for use in reinforcing mortar due to their availability and low market cost (37). According to the Food and Agriculture Organization (FAO) report of 2023, global jute production reached 2973.1 thousand tonnes in 2021/22, with Asia being the epicenter of this industry, contributing approximately 99.7% of this total. In the jute plant, each part is utilized significantly: the outer layer is used for fiber production, the inner stem is utilized in papermaking, and even the leaves are used as edible food. Jute is also extensively cultivated in Brazil and has adapted well to the tropical equatorial climate of the Amazon (43, 44).

The natural fiber textile market anticipates significant growth, with an estimated rate of 7.40% during the period from 2021 to 2028. This increase is driven by the growing use of these fibers as substitutes for synthetics, along with the increasing concern to reduce the use of plastic materials in regions such as Europe and North America. Other factors include the abundant availability of raw materials, expansion of end-user industries, and the development of advanced technologies in fiber production. Demand is also being boosted by the manufacturing of advanced natural fiber composites, which are widely used in automotive interiors. This trend offers lucrative opportunities for participants in the natural fiber textile market during the forecast period until 2028 (45).

The fibers used were obtained from the city of Coari, in the Brazilian Amazon region, specifically from Coari – AM, in long bundles, as depicted in Figure 1. In the laboratory, the fibers were aligned and cut into lengths of 40 mm. Subsequently, an alkaline treatment was applied to the jute fibers to reduce water absorption and enhance the fiber-matrix adhesion. The treatment followed the method presented by Ferreira et al. (34): the fibers were immersed in a solution of $\text{Ca}(\text{OH})_2$ at a controlled laboratory temperature (23°C) with a concentration of 0.73% of the fiber weight for 50 minutes. Afterward, they were dried in a chamber with forced air flow at 40°C for 72 hours.



FIGURE 1. Processing and alkaline treatment of jute fibers.

2.1.2. Test Methods

The evaluation of the effect of jute fiber treatment on morphology, structure, and physical and mechanical properties was conducted using scanning electron microscopy (SEM), X-ray diffraction (XRD), direct tensile testing, and water absorption analysis.

A Hitachi TM4000 Plus tabletop microscope was utilized to perform scanning electron microscopy (SEM) to investigate the jute properties at a microscopic level. It was also used to calculate area measurements using magnified images of the cross-section and fiber surface, employing ImageJ software. Jute fiber samples were soaked in water for 72 hours for swelling and then cut with steel blades to observe the cross-section before drying in a hot air room at 40°C for 48 hours.

X-ray diffraction (XRD) analyses were carried out using a Bruker D8 Focus diffractometer. The diffracted radiation intensity was measured within a range of 2θ between 10° and 40° with a step size of 0.05° at $3^\circ/\text{min}$. For sample preparation, fibers were cut into lengths shorter than 1 mm using scissors. From the X-ray spectrum, the crystallinity indices of natural and treated fibers were calculated.

The tensile tests were conducted using a Tytron 250 microforce testing machine with displacement control at a deformation rate of 0.005 mm/min. Fiber samples measuring 20 mm, 30 mm, and 40 mm for both treated and untreated fibers were glued onto a paper mold to maintain alignment in the testing machine, following the guidelines of ASTM C1557 (46). By utilizing SEM images, it was possible to calculate the fiber area to obtain the tensile strength.

The water absorption of jute fibers was carried out on samples weighing 1g and having a length of 40 mm, following this procedure: i) the fibers were dried in an oven at 80°C until a constant mass was achieved, and after 48 hours, the dry mass of each sample was determined. ii) The fibers were immersed in water, and the wet mass was determined using an electronic balance with the aid of absorbent paper to remove excess water from the samples. iii) The determination of the wet mass was carried out at intervals of 3 hours, 6 hours, 24 hours, 48 hours, and 72 hours. Eight samples were selected for a better assessment of water absorption of the fibers, divided into 4 reference samples and 4 treated samples. The calculation used for the percentage of water absorption was as follows:

$$A = \left(\frac{M_s - M_d}{M_d} \right) \quad [1]$$

where M_s is the wet mass at each time interval, and M_d is the initial dry mass of each sample.

2.2. Short Jute fiber reinforced mortar (SJFRM)

2.2.1. Materials

To produce SJFRM, the binder consisted of a ternary blend comprising 50% by mass of Portland cement CPIIF, with a specific mass of 3.05 g/cm³, 20% of fly ash, with a specific mass of 2.15 g/cm³, and 30% of metakaolin, with a specific mass of 2.15 g/cm³.

The chemical composition of the materials is presented in Table 1. Fly ash and metakaolin can be classified as pozzolans according to ASTM C618-03 (47), since the sum of three oxides from their chemical analyses, SiO₂+Al₂O₃+Fe₂O₃, was higher than 70%.

Thermogravimetric (TG) analysis was conducted on blended cement paste after 28 days of curing using the SDT Q600 TGA/DTA/DSC equipment from TA Instruments. The absence of an exothermic peak between temperatures of 400 °C and 450 °C demonstrates that the cement paste does not contain free calcium hydroxide, ensuring the durability of the vegetable fibers (48).

TABLE 1. Chemical composition of binders.

Component	Cement (%)	Fly ash (%)	Metakaolinite (%)
CaO	67.94	2.11	-
Al ₂ O ₃	2.94	32.89	46.01
SiO ₂	10.31	50.28	39.45
TiO ₂	0.30	1.57	1.84
SO ₃	2.94	1.46	1.11
Fe ₂ O ₃	3.98	5.96	7.28
K ₂ O	0.37	3.94	-
Others components	0.43	0.28	0.95
Fire loss	10.78	1.51	3.36

The fine aggregate used was natural river sand with a passing fraction through sieve #600 microns, having a specific mass of 2.67 g/cm³ and a fineness modulus of 1. To enhance workability and reduce matrix

segregation, a superplasticizer additive (SP) based on polycarboxylate polymers, Glenium 51, of the polycarboxylate ether type manufactured by BASF, and a viscosity-modifying agent (VMA), Rheomac UW 410 manufactured by BASF with a density of 0.31 g/cm³, were employed.

The consumption per cubic meter of materials used in the production of the mortars is presented in Table 2.

2.2.2. Characterization methods

The JFRM were analyzed in their fresh state to assess their workability, employing the standard consistency test specified by ABNT NBR 13276 (49). Additionally, the determination of bulk density in the fresh state was carried out in accordance with ABNT NBR 13278 (50).

Water absorption was conducted following the ABNT NBR 9778 standard (51). Four cylindrical specimens (50 mm x 100 mm) were molded for each mortar mixture.

Direct compression testing was performed on four cylindrical samples of 50 mm in diameter and 100 mm in height for each mixture, at 28 days. A Shimadzu AGX -100 kN testing machine was used at a speed of 0.3 mm/min. Displacements were measured by two LVDTs attached to the central region of the specimen. The modulus of elasticity was determined according to ASTM standards. For the four-point bending test, specimens of 400 mm x 80 mm x 14 mm were molded, with a free span of 300 mm and a distance between loads of 100 mm.

The test was conducted using a Shimadzu AGX -100 kN testing machine at a speed of 0.3 mm/min, at 28 days. From the bending test, the stress and toughness were determined. The toughness index (TI) was calculated using the relationship between the area under the stress-deflection curve for different displacements (1 mm, 2 mm, 4 mm, 6 mm, and 10 mm) divided by the area under the curve up to the displacement related to the appearance of the first crack.

2.3. Assessment of masonry walls

2.3.1. Manufacturing of wall prototypes

For the evaluation of masonry, samples of dimensions 60 x 60 x 9 cm³ were produced using blocks with

TABLE 2. Mix proportions (kg/m³).

Mix ID	Cement	FA	Metakaolin	Sand	Water	SP	Fiber	VMA
J0	402.51	161.01	241.51	805.03	402.51	4.03	-	-
J2	397.59	159.04	238.55	795.18	397.59	19.88	15.90	1.19
J3	395.17	158.07	237.10	790.35	395.17	31.61	23.71	1.42

holes in the horizontal position, as shown in Figure 2. The specified dimensions differ from those mentioned in ASTM E519/E519M-15 (47) for adjusting the test in the laboratory testing machine. However, the prisms follow a standard designated for height and length that are equal. The change in masonry prism dimensions for diagonal compression tests has already been considered in other works on the subject. For instance, Sandoval et al. (22) used panels with a standard of 86 x 85 cm for diagonal compression tests; Madhavi et al. (52) produced prisms of 70 x 70 cm, Lee et al. (53) produced prisms of 19 x 19 cm, and Arisoy et al. (54) produced prisms of 50 x 50 cm.

Ceramic bricks measuring 29 cm x 19 cm x 9 cm, with 10 holes (Figure 3), were used and subjected to a direct compression test according to ABNT NBR 15270-3 (55). Ten masonry samples were tested, which were faced with mortar for surface regularization. The compression strength obtained, 1.0 ± 0.2 MPa, indicates that the blocks can only be used in partition walls.

A 10 mm-thick mortar was applied in the joints between the blocks (Figure 2), prepared with a mass ratio of 1:0.5:2:1 (cement, hydraulic lime, sand, and water). The assessment of this mortar used in the masonry joints exhibited a compression strength of 6.4 ± 0.4 MPa after 28 days.

The production and application process of the rendering mortar are illustrated in Figure 4. Following the construction of the block wall, a first thin layer of mortar (approximately 5 mm thick), without fibers, was applied using a trowel on the moistened masonry surface to enhance adhesion (Figure 4b). After 14 days from the construction of the masonry wall, the JFRM was prepared in a 20 dm³ bench mount (Figure 4c) and manually applied (Figure 4d) until reaching a total thickness of 20 mm on each side of the wall (Figure 4e). To ensure the perfect hydration of the cement

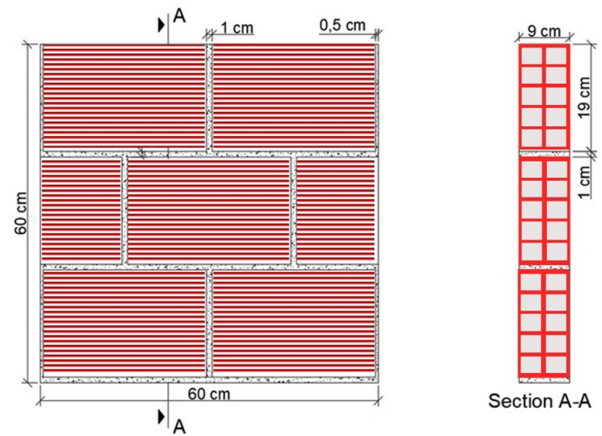


FIGURE 2. Configuration and dimensions of uncoated walls.

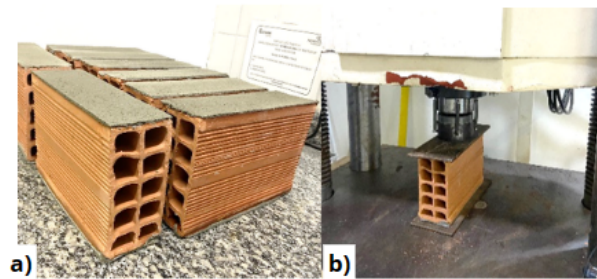


FIGURE 3. Testing of ceramic blocks in accordance with ABNT NBR 15270-3 (55). a) regularization of blocks, b) test setup.

paste and prevent the emergence of drying shrinkage cracks, the walls were covered with a damp cloth for 3 days after completing the coating. Table 3 presents the identification of each prism produced.

The walls were air-cured within the laboratory premises until the date of testing (Figure 4f).



FIGURE 4. Production of wall samples. a) construction of hollow brick masonry, b) roughcasting, c) preparation of rendering mortar, d) application of rendering mortar, e) finishing and smooth surface, and f) curing.

TABLE 3. Wall samples.

Identification	Fiber content of coating layer (%)	Final size of masonry wallet (cm)
WJ0	0	
WJ2	2	60 x 60 x 12
WJ3	3	

2.3.2. Diagonal compression test

The diagonal compression test is widely used to investigate the strength within the plane of masonry prisms, as the failure mode of the specimens resembles that induced by lateral seismic and wind forces. Diagonal compression generates a combined state of shear and compression along the horizontal and vertical joints. The method involves applying compressive force at two diagonal corners to replicate these conditions, and the loads must be carefully designed (16, 52).

The ASTM E519/E519M-15 standard (56) provides the most used methodology for conducting diagonal compression tests and calculating the shear stress of wall prisms based on the effective cross-sectional area. The diagonal compression test was conducted at 28 days on each wall using a Shimadzu universal testing machine of 200 kN capacity and at a displacement rate of 0.3 mm/min, as shown in Figure 5a. Displacements were measured using two LVDTs positioned horizontally and vertically, as depicted in Figure 5b.

According to ASTM E519/E519M-15 (56), the

shear stress is given by:

$$\tau_{ASTM} = 0.707 \cdot \frac{P_{max}}{A_n} \quad [2]$$

where P_{max} is the maximum applied load, and A_n is the effective cross-sectional area, calculated as follows:

$$A_n = (w + h^2) \cdot t \cdot n \quad [3]$$

where w is the width of the masonry prism, h is the height of the masonry prism, t is its thickness and n is the percentage of the gross area of the brick.

The RILEM-TC-76-LUM standard (57) proposes the calculation of shear stress using Equation [4]:

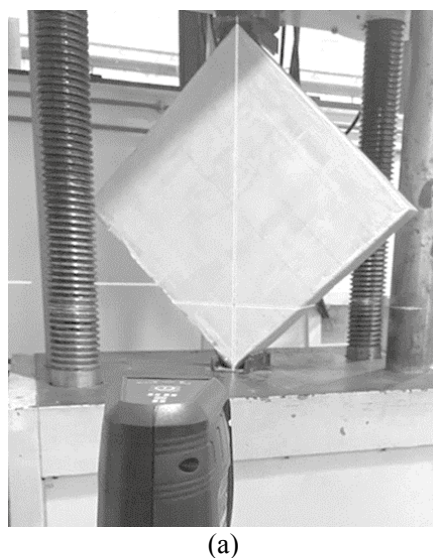
$$\tau_{RILEM} = 0.88 \cdot \frac{P_{max}}{A_n} \quad [4]$$

The transverse strain modulus is determined by ASTM E519/E519M-10 (56) using Equations [5] and [6]:

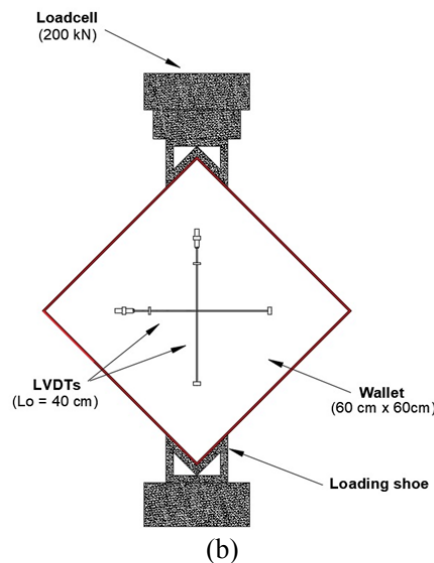
$$G = \frac{\tau_{ASTM}}{\gamma} \quad [5]$$

$$\gamma = \frac{\Delta x + \Delta y}{L_o} \quad [6]$$

where τ is the shear stress given by Equation [2], γ is the total deformation (mm/mm), Δx is the vertical displacement (mm), Δy is the horizontal displacement (mm) and L_o is the initial distance between the displacement measurement points (mm).



(a)



(b)

FIGURE 5. Configuration of the diagonal compression test. a) alignment with laser sight, b) support devices and LVDTs.

3. RESULTS AND DISCUSSION

3.1. Effect of treatment on the properties of jute fibers

The jute fibers are formed by an irregular aggregation of fibrocells containing a central channel (lumen) inside them. Some modifications were observed in the morphology of jute fiber after alkaline treatment. Images obtained by SEM, shown in Figures 6 and 7, revealed a reduction in the cross-section with a change in fiber diameter and closure of some lumens. Additionally, the lateral surface was damaged by the fiber treatment, resulting in the appearance of lateral cracks due to delamination between the fibrocells, as previously observed by Jo et al. (35) after alkaline treatment. Moreover, deposits of calcium hydroxide crystals of varying dimensions were found on the surface of the treated fiber, which, coupled with increased roughness, could contribute to increased fiber-matrix adhesion (31, 58, 59).

The effect of alkaline treatment on the morphology of fibers, with the closure of lumens (33), directly results in the reduction of the fibers' water absorption capacity. Vegetable fibers typically display substantial water absorption, particularly in the initial immersion hours due to a significant volumetric

presence of permeable voids (60). Following 3 hours of immersion, the untreated fiber exhibited a water absorption rate of 158.77%, while the treated fiber absorbed 149.90%. After 72 hours, natural jute fiber demonstrated an absorption rate of 272.74%, whereas the treated fiber absorbed 224.11%. Cottrell et al. (61) illustrated that their study's untreated jute fibers absorbed 205% within the first 50 minutes, maintaining a similar range throughout the total observation time of 90 minutes. Comparable trends were observed in other fibers, with average absorptions surpassing 150%, varying according to the observation period, such as sisal fibers (62), pineapple leaf, sisal, and jute fibers (33).

In addition to modifying the lumens, alkaline treatment leads to the partial removal of lignin and surface impurities (63), which are hydrophilic components of the fiber (hydroxyl groups - OH) with greater water absorption capacity. Indeed, the crystallinity index (CI) obtained from X-ray diffraction analysis, shown in Figure 8, indicates that the natural fiber had a CI value of 60.75%, consistent with findings in other studies (64, 65), while the fiber subjected to alkaline treatment showed a CI value of 66.22%. This increase, corresponding to a 9% rise in crystallinity, aligns with the reduction of impurities and lignin in the fiber, while preserving cellulose (66).

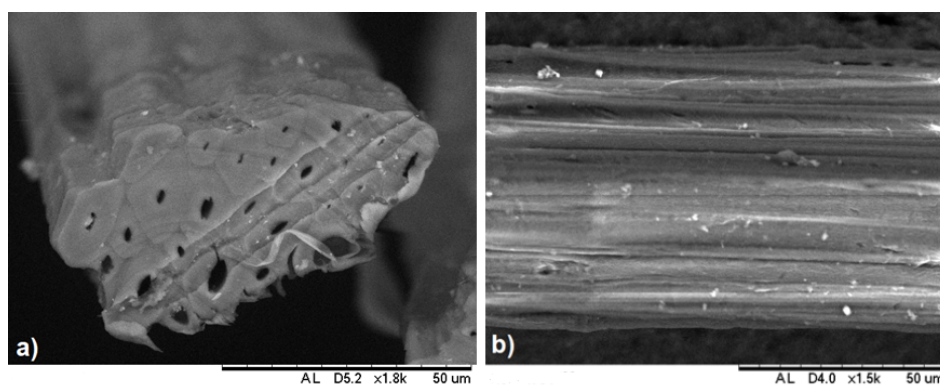


FIGURE 6. Microscopy images of natural fibers. a) cross section, b) lateral surface.

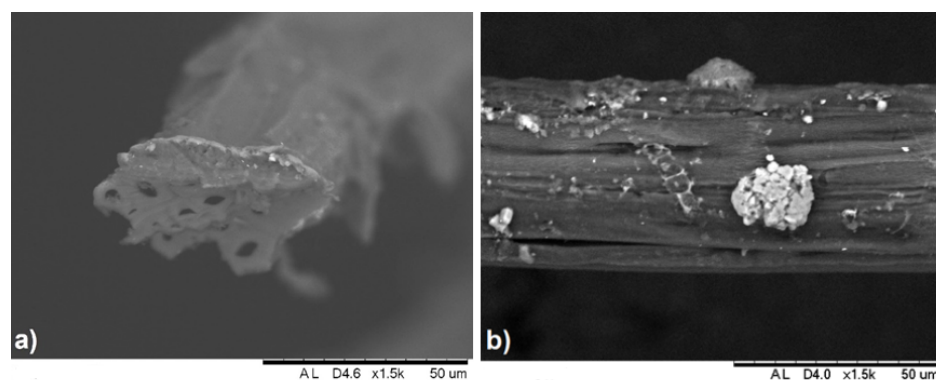


FIGURE 7. Microscopy images of treated fibers. a) cross section, b) lateral surface.

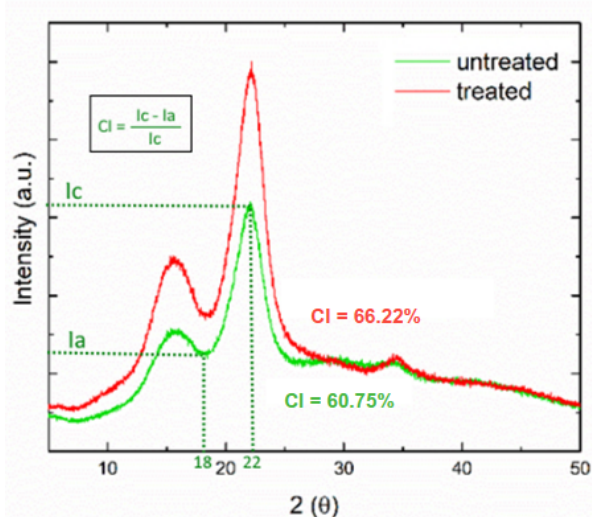


FIGURE 8. Crystallinity of jute fibers.

Figure 9 illustrates stress-strain curves depicting the tension testing of both natural and treated jute fibers. Their typical behavior demonstrates linear elasticity until a sudden, brittle rupture occurs. The values for tensile strength, rupture deformation, and modulus of elasticity presented in Table 4 were obtained from these curves.

The tensile strength and elastic modulus were improved in 25% and 23%, respectively, with alkaline

treatment. According to Sinha and Rout (67), the improvement in mechanical strength and elasticity modulus is attributed to a structural transformation induced by alkaline treatment. In natural jute fibers, hemicelluloses and lignin persist in the inter-fibrillar region, imposing constraints on the cellulose chains, thereby keeping them separate.

The removal of hemicelluloses and lignin during alkaline treatment alleviates this internal constraint, enabling the fibrils to undergo reorganization. This densification of the cellulose chains contributes significantly to the enhancement of overall mechanical properties. The increase in the crystallinity index following treatment supports this hypothesis. Comparable outcomes, demonstrating increased jute fiber tensile strength, were observed by others researches (5, 30, 33, 68), following alkaline treatment of jute.

3.2. Short jute fiber reinforced mortar (SJFRM)

Mortars reinforced with 2% and 3% of treated jute fibers, denoted as J2 and J3, respectively, underwent a consistency test (flow table test) to assess workability compared to the fiber-free mortar (J0). Figure 10a presents the values obtained in the test and the consistency reduction observed upon fiber introduction. There is a reduction of 2.04% and 12.24% in consistency, concerning J0, for the J2 and J3 mortars, respectively.

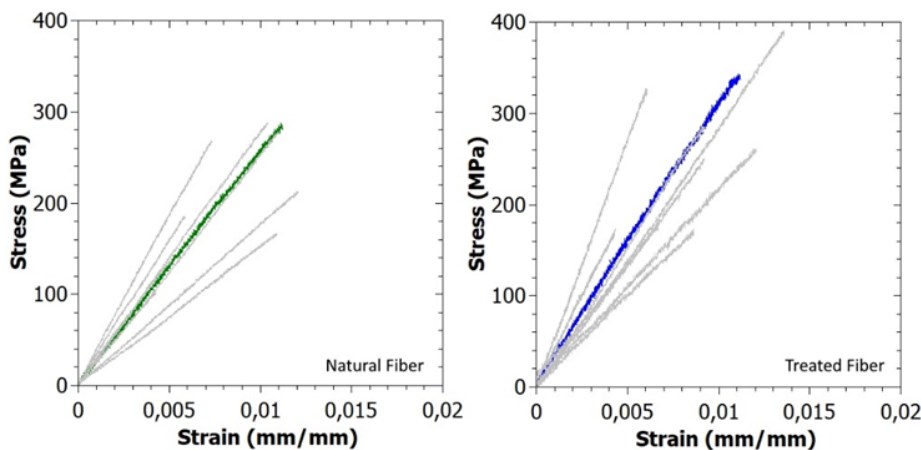


FIGURE 9. Typical tensile behavior for natural and treated fibers.

TABLE 4. Mechanical properties of fiber.

Treatment	Tensile strength (MPa)	Rupture deformation (mm/mm)	Elastic modulus (GPa)
No treatment	186.44 ± 53.58	0.0083 ± 0.0029	23.32 ± 6.05
Alkaline	250.78 ± 57.99	0.0063 ± 0.0017	30.29 ± 9.21

This reduction in workability upon fiber addition, also observed by other authors (39), is associated with water loss from the mixture that is rapidly absorbed by the jute fiber due to its high water absorption capacity. Additionally, it involves disturbance in the flow of the mixture due to the presence of fibers, which create friction with the aggregate and tend to entangle, forming clusters within the mixture and increasing the content of entrapped air. As a consequence, there is a reduction in density in the fresh state, as shown in Figure 10b. The addition of 2% and 3% of fibers resulted in reductions of 8.85% and 13.02%, respectively, compared to J0.

The assessment of water absorption, void ratio, and density of mortars in the hardened state confirms the effect of fiber addition on increasing internal porosity and water penetration capacity within the mortars, as depicted in Table 5. With the addition of 2% jute fibers, there is an approximately 49% increase in water absorption and a 50% rise in porosity. Conversely, for the J3 mortar with 3% fibers, the increase in porosity (around 56%) was higher than the observed water absorption (around 83%), indicating that the added fibers create internal voids that are not accessible to water.

The elevation in porosity in fiber-reinforced composites is linked to the entrapment of voids during the mortar production process, given the reduced workability,

resulting in greater difficulty in homogenizing the components and in casting into molds. Even in small volumes compared to the matrix, the fibers still contribute to reducing porosity and increasing water absorption in the hardened mortar. This is because the fibers introduce preferred pathways for water movement within the structure. The introduction of fibers led to a decrease in the density of the mortars, although the maximum reduction of 5%, concerning J0, is not proportional to the reduction in porosity.

Table 6 displays the results of the mechanical characterization of the mortars. The compressive strength and modulus of elasticity of the mortars decreased with the increase in fiber content. Compared to J0, there was a reduction of 7.3% and 22.3% in compressive strength, and a reduction of 6.5% and 13.9% in modulus of elasticity with the addition of 2% and 3% of fibers, respectively. The result confirms the inversely proportional relationship between porosity and the mechanical strength of solid materials, as the addition of fibers led to greater air incorporation into the mortar structure. However, due to the use of a more fluid mixture with a high content of fines, it is observed that the decrease in compressive strength was less severe than that reported by Majumder et al. (38) for mortar with 2% jute fibers, which showed a drop in compressive strength of up to 41.37%.

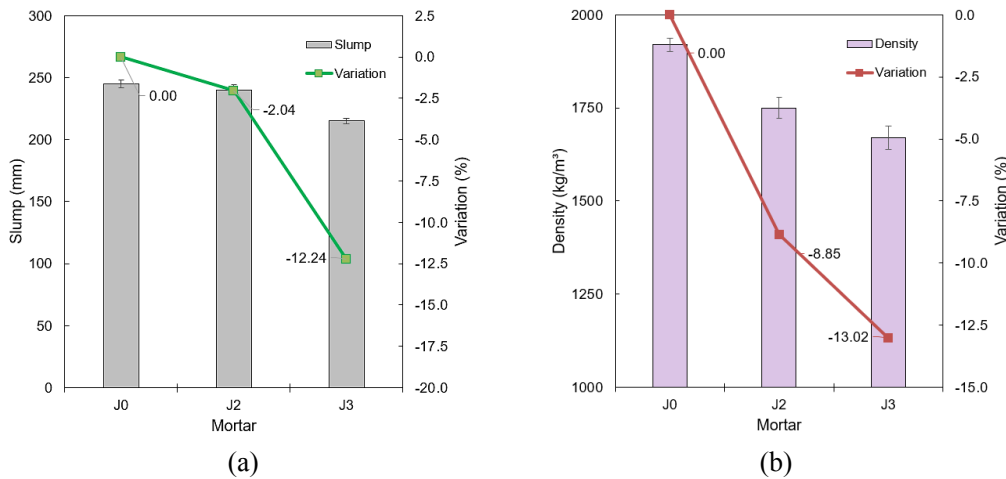


FIGURE 10. Fresh state of mortars. a) consistency, b) density.

TABLE 5. Physical characterization of mortars in the hardened state.

Mix ID	Water absorption (%)	Mass density (kg/m³)	Void index (%)
J0	7.41 ± 0.36	1812 ± 0.02	13.40 ± 0.41
J2	11.57 ± 0.83	1750 ± 0.02	20.19 ± 1.26
J3	14.31 ± 0.33	1714 ± 0.01	24.45 ± 0.42

TABLE 6. Results of mechanical tests.

Mix ID	Compressive Strength (MPa)	Young's Modulus (GPa)	Four-point flexural test			
			σ_f (MPa)	δ_f (mm)	σ_u (MPa)	δ_u (mm)
J0	35.16 ± 0.60	23.18 ± 3.10	3.39 ± 2.94	0.41 ± 0.04	-	-
J2	32.55 ± 1.43	21.67 ± 1.70	3.38 ± 0.25	0.39 ± 0.02	2.33 ± 0.47	3.23 ± 0.15
J3	27.32 ± 0.14	19.95 ± 2.61	2.91 ± 0.15	0.42 ± 0.02	2.49 ± 0.33	4.18 ± 0.34

The stress-strain curves obtained in the flexural test are shown in Figure 11. While the mortar J0 exhibited sudden failure after the appearance of the first crack, in the J2 and J3 mortars, a change in behavior under flexion is observed, with the maintenance of residual stress after cracking and an increase in rupture deformation. This leads to an increase in energy absorption capacity (material toughness). Before the appearance of the first crack, the mortars exhibit linear elastic behavior with minimal contribution from the fibers to the flexural strength or stiffness. When compared to the flexural strength of mortar J0, it's observed that the first crack stress remains unchanged with the addition of 2% of fibers, as indicated in Table 6. However, with the addition of 3% of fibers, there is a 14% reduction in flexural strength.

The post-cracking behavior is characterized by two main stages:

- i. following a sudden drop in stress due to the opening of the first crack, there is a process of internal

stress transfer by the fibers crossing the cracks, resulting in a gradual increase in stress. Depending on the content and distribution of the fiber reinforcement within the sample, a second crack may occur, accompanied by a new recovery of strength;

- ii. with the increase in internal stresses and the widening of the existing crack, there is a propagation of the crack at the fiber-matrix interface and a process of fiber pull-out from the interior of the matrix.

Consequently, the stress-displacement behavior becomes governed by the frictional adherence of the fiber, with a gradual reduction in stress and sliding of the fiber in the cracked region. The maximum residual stress σ_u presented in Table 6 indicates that the addition of 2% and 3% of fibers allows achieving post-cracking stresses of approximately 69% and 85% of the flexural strength, respectively, with deformation values 8 to 10 times higher than the peak deformation.

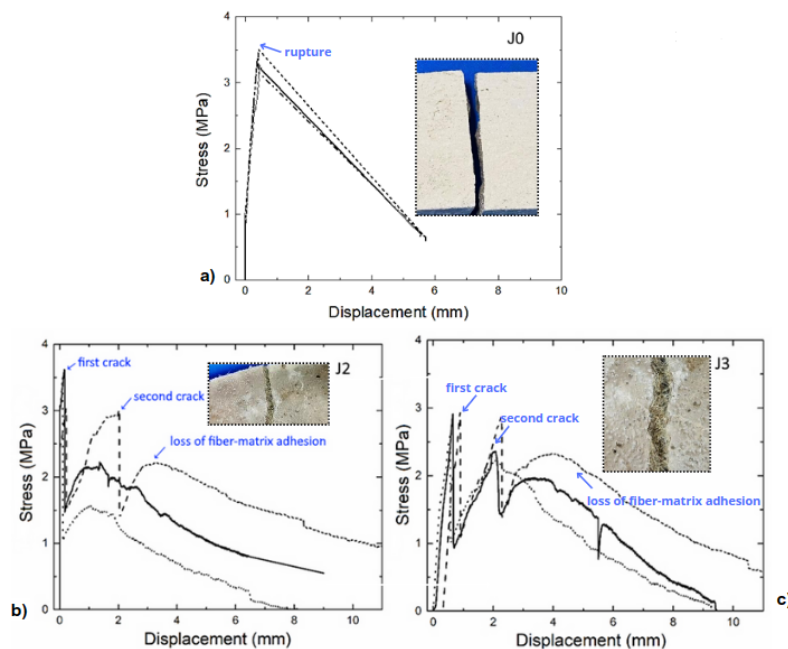


FIGURE 11. Stress x displacement curves under bending. a) J0, b) J2, c) J3.

As a result, the mortars demonstrate an increase in material toughness, as shown in Table 7. There is a variation of the toughness index (TI) of the J2 and J3 mortars with increasing displacement. It is observed that for displacements up to 2 mm, mortar J2 exhibits a greater increase in toughness compared to mortar J3. However, this behavior changes for larger displacements, with the higher fiber content being more decisive in stress transfer and the final fiber pull-out process. The fracture energy of fiber-reinforced mortars typically stands out in comparison to ordinary mortars, as their mechanical behavior becomes less brittle after cracking in the flexural test, with the mortars maintaining stability and shape (40). In this regard, jute fiber has positively influenced mechanical results to produce new materials (69).

3.3. Assessment of masonry walls

Figure 12 shows the typical load displacement curves obtained in the diagonal compression test of walls. The mechanical behavior of the walls is characterized by an approximately linear load-displacement relationship until the appearance of the first crack in the coating lay-

er. For the unreinforced wall J0, the maintenance of the cracking load is observed until a small displacement (of the order of 0.4 mm) with a sudden loss of strength. For the walls coated with SJFRM, on the other hand, the post-cracking behavior is followed by an increase in wall strength and higher rupture displacements. Table 8 presents the results of the maximum load for each tested wall sample, as well as the mean value and standard deviation. The shear stresses, calculated according to Equations [2] and [4] established by the ASTM E519/E519M-15 (56) and RILEM-TC-76-LUM (57) standards, are also presented. The area of the specimens was calculated based on Equation [3].

It is observed that the presence of short jute fiber as reinforcement in the coating mortar results in an increase of up to 41% in the shear strength of the walls. Increased shear strength of walls has also been achieved with the use of reinforcement in plant fabrics such as jute (52) or hemp (20). Like fabric reinforcement, the use of short fibers as wall reinforcement inhibits the propagation of the initial crack and, thus, modifies the failure mode (27). Figure 12 shows the load-displacement curves obtained in the diagonal compression test of walls coated with mortar without fibers (WJ0) and with mortar containing 2% (WJ2)

TABLE 7. Mortar toughness for different displacement values.

Mix ID	δ_f (mm)	Mortar toughness (N.m)				
		1 mm	2 mm	4 mm	6 mm	10 mm
J0	1.03 ± 0.09	-	-	-	-	-
J2	0.81 ± 0.18	1.94 ± 0.32	4.04 ± 0.94	7.12 ± 2.04	9.42 ± 3.39	11.95 ± 6.01
J3	0.71 ± 0.26	1.26 ± 0.20	3.09 ± 0.20	7.01 ± 0.21	10.13 ± 1.17	13.42 ± 4.16

TABLE 8. Results of shear stress in the walls.

Fiber content	Sample	Maximum Load (N)	Shear stress ASTM (MPa)	Shear stress RILEM (MPa)
No fiber	WJ0-1	41510	0.40	0.50
	WJ0-2	42800	0.42	0.52
	Average	42155 ± 912	0.41 ± 0.01	0.51 ± 0.02
2%	WJ2-1	41700	0.41	0.51
	WJ2-2	73293	0.72	0.90
	Average	57497 ± 22339	0.57 ± 0.22	0.70 ± 0.27
3%	WJ3-1	53514	0.53	0.65
	WJ3-2	64000	0.63	0.78
	Average	58757 ± 7414	0.58 ± 0.07	0.72 ± 0.09

and 3% (WJ3) of short jute fibers. The positive side shows the horizontal stretching of the prism, while the negative side shows the vertical shortening based on the prism deformation.

The WJ0 prisms reached maximum applied load forces around 42.1 kN, on average. The unreinforced specimens exhibited typical brittle failure behavior, consisting of an elastic phase until reaching the maximum load, followed by sudden failure in both samples, as shown in the curves in Figure 12a. During the test, detachment of the mortar coating from the units was observed, indicating low adhesion, along with diagonal cracks extending towards the edges of the specimens. Unlike the unreinforced prisms, the curves of the reinforced prisms, with 2% and 3% fibers, were characterized by a post-peak phase with load maintenance up to higher deformations. As the crack opening grows, there is a gradual reduction in load due to the fiber pull-out process in the crack region.

Evaluating the prisms reinforced with mortars containing 2% fibers, there was a greater difference in the maximum load obtained by each sample, WJ2-1 and WJ2-2, which obtained peak loads of 42 kN and 73 kN, respectively. The lower peak load of sample WJ2-1 resulted from the detachment between the masonry and the reinforcement layer at the point of load application, as shown in Figure 15. Wall WJ2-2, which reached the highest applied load among the studied walls, exhibited an initial crack with a load close to 50 kN, with a slight drop in load, followed

by a load increase up to 73 kN. After the peak load, there is an abrupt reduction in load, with continued horizontal deformation and a tendency for cracking, both diagonal and horizontal, near the application of the test load. This occurs mainly in the reinforced specimens, where there is a greater accumulation of stresses (70).

The effect of applying mortar with 3% of fibers can be observed in Figure 12c. Specimens WJ3-1 and WJ3-2 exhibited peak loads of 53 kN and 64 kN, respectively. In prism WJ3-1, delamination was observed between the coating and the ceramic block near the lower load application shoe, along with horizontal cracks that appeared in the blocks after reaching the maximum load. There was also rupture between the block-coating in contact with the crack region. Small cracks at the top and bottom of the prism were caused by tensile forces. Sample WJ3-2 exhibited small diagonal cracks, attributed to diagonal/shear compression forces. Despite the crushing of the blocks near the load application, there was significant maintenance of wall stability even after the end of the test.

It is important to highlight that the dimensions of the prisms used in the tests were smaller than those prescribed by ASTM E519/E519M-15 (56), which may have influenced the mode of failure, especially at the support and load application points. As a result, the obtained results may be more conservative than those obtained in larger samples. Typically, larger samples have a higher probability of defects. In addi-

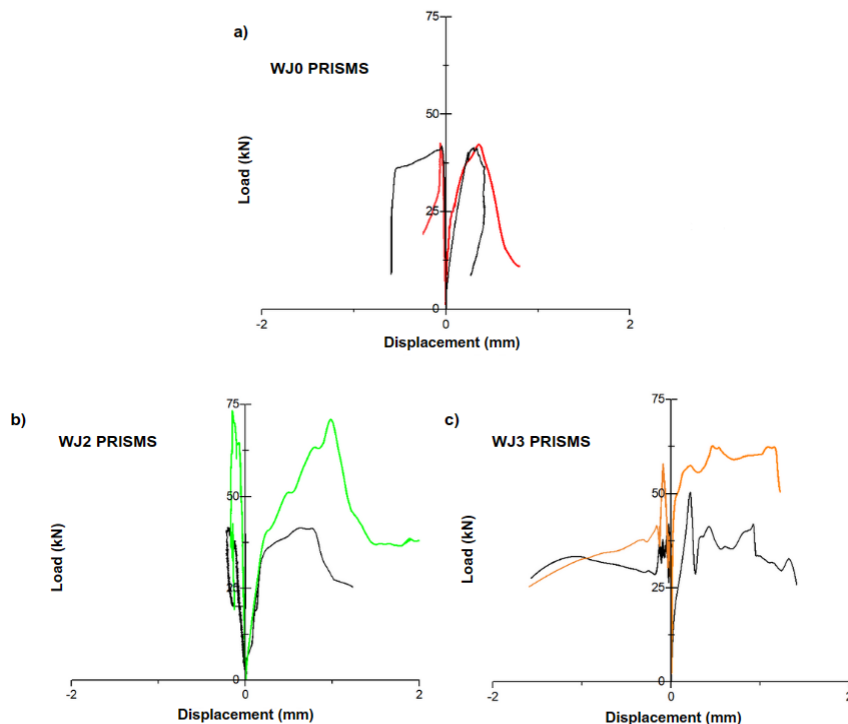


FIGURE 12. Typical load displacement curves obtained in the diagonal compression test: a) WJ0 prisms, b) WJ2 prisms, c) WJ3 prisms.

tion, the presence of a larger number of blocks in the sample influences the results because, according to Yu et al (71), the contribution of the wall coating layer to mechanical resistance is influenced by the integrity of each component of the system. Samples smaller than those established by the standard have been frequently used by some researchers due to equipment limitations or for ease of execution and handling (22, 52, 53, 54).

The unreinforced walls, under diagonal compression test, presented vertical cracking from the point of load application, which is common for this type of test, as shown in Figure 13. This shear failure mode, already identified by other authors (72, 13), occurs when the principal tensile stress developed internally in the wall exceeds the tensile strength of the masonry components, including the coating (73).

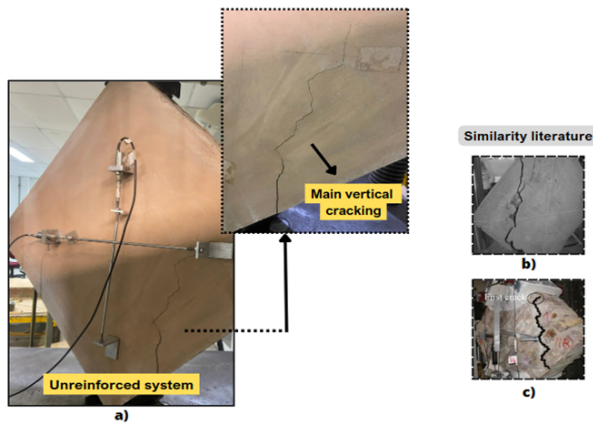


FIGURE 13. Failure of walls without fibers and comparison with the literature. a) WJ0 prisms (without fibers), b) Mezrea et al. (72), c) Sherny; Dubeo (13).

Figure 14 depicts the failure mode of walls reinforced with short jute fibers, identified as toe crushing, which is a result of wall crushing under compression (toe compression failure). In this case, initial arched cracking is observed below the loading apparatus and roughly transverse to the loading direction. With increasing loading, a vertical crack appears, and the ceramic block is crushed by the support apparatus. Laterally, the crack propagates between the wall and the coating, with the fibers acting to inhibit crack propagation, as shown in Figure 14b. Figure 14c illustrates the crack propagation on the other side of the wall.

After reaching the maximum load, the mechanical behavior of walls reinforced with fibers is characterized by a gradual loss of load-bearing capacity and the simultaneous formation of various failure mechanisms, as shown in Figure 14. In addition to coating cracking, detachment between the coating and the ceramic blocks was observed, as reported by Mezrea et al. (72), and the rupture of the ceramic block. The

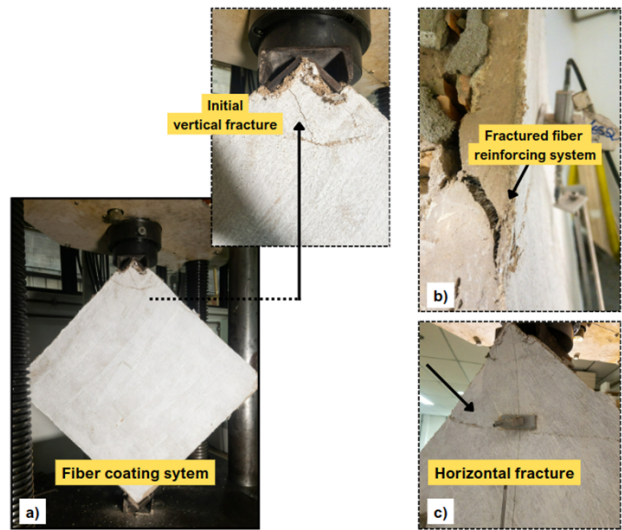


FIGURE 14. Cracking pattern of walls coated with mortars reinforced with jute fiber. a) initial vertical fracture in fiber coating system, b) fractured fiber reinforcing system, c) horizontal fracture in fiber coating system.

characterization results demonstrate that the ceramic block has a compressive strength lower than that of the coating mortar and the mortar used in the joints, making it the component most susceptible to cracking and rupture, as shown in Figure 15b and 15d, due to crushing under compression at the load application point.

Four failure mechanisms of walls coated with mortar reinforced with jute fibers, both with 2% and 3% fibers, were more notably encountered in the diagonal compression tests. Based on Figure 15, the following are identified in the samples:

- Detachment at the interface of the reinforcement mortar with the masonry substrate, i.e., between the plaster-coating-bricks. Caused by the loss of adhesion between the materials, as shown in Figure 15a;
- Emergence of cracks in the ceramic block used, which had much lower resistance than the other materials used (mortar for laying and the produced coating mortar), resulting in vertical and/or horizontal cracks (Figure 15b). Points of fragility are observed in the walls due to the heterogeneity of the materials, as in the case of the bricks;
- Emergence of cracks near the steel shoe, in lower or upper contact, near the application of load. There was also a tendency for fiber pullout in these regions (Figure 15c);
- Crushing of the bricks (Figure 15d). There is a mechanism of failure development in the region near the steel shoes that implies the emergence of several cracks both in the coating mortar and in the bricks. The cracks that appear through the bricks led to their total rupture (by crushing) at some moments.



FIGURE 15. Failure modes of the test specimens. a) detachment of the plaster, b) cracks in the bricks, c) cracks in the masonry in contact with the footing, d) crushing of the brick.

It is observed, therefore, that the presence of fiber reinforcement inhibits crack propagation in the coating, modifying the wall failure mode, which is now controlled by the strength of the ceramic block and the wall-coating adhesion. For this reason, the fiber con-

tent used as reinforcement does not affect the maximum shear stress of the walls, as there was control of microcracking, and the coating was not brought to rupture. Overall, there is a significant contribution of the composite material in applications such as rendering mortar, maintaining masonry stability even after cracking. This indicates the potential of this type of mortar for retrofitting, resulting in crack control and failure mode as already observed by Khaleel; Madhavi and Basutkar (74) and Dong *et al.* (75).

The presence of fibers inhibits the propagation of initial cracks in the coating, resulting in a reduction of axial and transversal deformations. Table 9 presents the deformation coefficient (γ) found and the transversal deformation modulus (G) of each wall, based on Equations [5] and [6]. The values of vertical shortening Δx and horizontal elongation Δy were obtained considering the elastic phase up to the first crack of the samples.

Based on Table 9, it is observed that the deformation modulus was enhanced for walls with jute reinforcement in the composition of the coating mortar. The results presented here confirmed the increased capacity of fiber-reinforced walls to resist elastic deformation throughout the application of load. This also resulted in an increase in the stiffness of these walls, as observed in Figure 12, with the continuity of deformation during the plastic phase of the material still under load. The deformation coefficients showed increases around 2 and 3 times higher for 2% and 3% of fibers, respectively, compared to the unreinforced wall (WJ0).

TABLE 9. Deformation and transverse deformation modulus results.

Fiber content	Sample	Δx (mm)	Δy (mm)	$\gamma 10^{-4}$ * (mm/mm)	G (GPa)
No fiber	WJ0-1	-0.067	0.379	7.81	0.54
	WJ0-2	-0.049	0.305	6.42	0.62
	Average	-0.06 ± 0.01	0.34 ± 0.05	7.11 ± 0.98	0.58 ± 0.06
2%	WJ2-1	-0.178	0.520	8.55	0.50
	WJ2-2	-0.090	0.255	4.12	1.75
	Average	-0.13 ± 0.06	0.38 ± 0.18	6.33 ± 3.13	1.13 ± 0.88
3%	WJ3-1	-0.082	0.232	3.76	1.41
	WJ3-2	-0.103	0.218	2.90	2.17
	Average	-0.09 ± 0.01	0.22 ± 0.01	3.33 ± 0.61	1.79 ± 0.54

*Deformation modulus calculated based on the shear stress according to ASTM E519/E519M-15 (56).

The positive results obtained with the application of fiber-reinforced mortars, when compared to conventional mortar reinforcement, indicate the great potential of this technique for retrofitting. Compared to the TRM reinforcement technique, the application of fiber-reinforced mortar is faster and easier to apply and requires less labor, as it does not require placement of the mesh over the masonry.

4. CONCLUSION

The study investigated the characteristics of coating mortars incorporating jute fibers to assess the shear behavior of ceramic block masonry. The key findings are summarized as follows:

- Alkaline treatment significantly enhanced the tensile strength and elastic modulus of jute fibers.
- Water absorption of fibers impacted mortar rheology, resulting in a 12% reduction in mortar consistency with 3% fiber. However, the consistency remained sufficient for masonry coating applications with up to 3% fiber volume.
- While compressive and flexural strengths tended to decrease with the addition of jute fibers, the stability of samples was maintained after the first crack. Jute fibers improved maximum deflection and increased displacement capacity and energy consumption.
- Mortars with 2% and 3% fiber demonstrated enhanced capacity to withstand stresses in diagonal compression tests, achieving considerably higher maximum applied loads than the non-reinforced system. Diagonal compressive strength increased by 28-30% compared to the unreinforced system.
- Shear stress in the non-reinforced system was 0.41 MPa. The reinforced system exhibited increased shear stress, reaching 0.57 MPa and 0.58 MPa for mortars with 2% and 3% fiber, respectively, comparable to similar systems in the literature.
- Reinforced walls showed increased elastic deformation resistance during load application, with deformation coefficients approximately 2 and 3 times higher for 2% and 3% fibers, respectively, compared to unreinforced walls.
- The results indicate that hollow clay brick masonry is more vulnerable to damage due to the low compressive strength of the material. But the strength of the mortar with fibers did a good job of not collapsing the construction system.

Jute fibers demonstrated potential for strengthening the analyzed walls. Further studies on the behavior of fiber-reinforced mortars in samples with larger dimensions or in different types of masonry, such as solid brick masonry or concrete bricks, are needed to confirm mortar reinforced with short jute fibers as a sustainable and efficient alternative for masonry reinforcement applications. In this study, the prisms un-

der compression had dimensions smaller than those prescribed by ASTM E519/E519M-15 (56), which may have influenced the results, notably the crushing observed at the load application points.

Funding sources

The authors would like to thank CAPES and CNPq for promoting and supporting the research. The second author thanks CNPq for the postdoctoral fellowship (Grant number 102164/2022-3).

Authorship contribution statement

Lidiane do Nascimento Farias: Conceptualization, Data curation, Formal analysis, Investigation, Validation, Research, Visualization, Writing – original draft, Writing – review & editing.

Paulo Roberto Lopes Lima: Conceptualization, Formal analysis, Methodology, Project administration, Visualization, Writing – review & editing.

Romildo Dias Toledo Filho: Conceptualization, Funding acquisition, Methodology, Project administration, Resources, Writing – review & editing.

Declaration of competing interest

The authors of this article declare that they have no financial, professional or personal conflicts of interest that could have inappropriately influenced this work.

REFERENCES

1. Qamar F, Thomas T, Ali M. 2019. Assessment of mechanical properties of fibrous mortar and interlocking soil stabilised block (ISSB). for low-cost masonry housing. *Mater. Construcc.* 69(336):e201. <https://doi.org/10.3989/mc.2019.13418>.
2. Choi Y, Park D, Kim S, Hong J. W. 2022. Seismic performance of crack-damaged masonry wall structures via shaking table tests. *Struct.* 45:2272-2291. <https://doi.org/10.1016/j.is-truc.2022.09.120>.
3. Yardim Y, Lalaj O. 2016. Shear strengthening of unreinforced masonry wall with different fiber reinforced mortar jacketing. *Constr. Build. Mater.* 102(1):149-154. <https://doi.org/10.1016/j.conbuildmat.2015.10.095>.
4. Petry S, Beyer K. 2015. Limit states of modern unreinforced clay brick masonry walls subjected to in-plane loading. *Bull Earthquake Eng.* 13:1073-1095. <https://doi.org/10.1007/s10518-014-9695-9>.
5. Khorasani FF, Kabir MZ. 2022. Experimental study on the effectiveness of short fiber reinforced clay mortars and plasters on the mechanical behavior of adobe masonry walls. *Case Stud. Constr. Mater.* 16:e00918. <https://doi.org/10.1016/j.cscm.2022.e00918>.
6. Vintzileou E, Miltiadou-Fezans A. 2008. Mechanical properties of three-leaf stone masonry grouted with ternary or hydraulic lime-based grouts. *Eng. Struct.* 30(8):2265-2276. <https://doi.org/10.1016/j.engstruct.2007.11.003>.
7. Kalagri A, Miltiadou-Fezans A, Vintzileou E. 2010. Design and evaluation of hydraulic lime grouts for the strengthening of stone masonry historic structures. *Mater Struct.* 43:1135-1146. <https://doi.org/10.1617/s11527-009-9572-1>.

8. Jorne F, Henriques FMA, Baltazar LG. 2014. Evaluation of consolidation of grout injection with ultrasonic tomography. *Constr. Build. Mater.* 66:494-506. <https://doi.org/10.1016/j.conbuildmat.2014.05.095>.
9. Isfeld AC, Moradabadi E, Laefer DF, Shrive NG. 2016. Uncertainty analysis of the effect of grout injection on the deformation of multi-wythe stone masonry walls. *Constr. Build. Mater.* 126:661-672. <https://doi.org/10.1016/j.conbuildmat.2016.09.058>.
10. Valluzzi MR, Binda L, Modena C. 2005. Mechanical behaviour of historic masonry structures strengthened by bed joints structural repointing. *Constr. Build. Mater.* 19(1):63-73. <https://doi.org/10.1016/j.conbuildmat.2004.04.036>.
11. de Santis S, Ceroni F, de Felice G, Fagone M, Ghiassi B, Kwiecień A, Lignola GP, Morganti M, Santandrea M, Valluzzi MR, Viskovic A. 2017. Round Robin Test on tensile and bond behaviour of Steel Reinforced Grout systems. *Compos. B. Eng.* 127:100-120. <https://doi.org/10.1016/j.compositesb.2017.03.052>.
12. de Santis S, de Felice G. 2015. Steel reinforced grout systems for the strengthening of masonry structures. *Comp. Struct.* 134:533-548. <https://doi.org/10.1016/j.compstruct.2015.08.094>.
13. Shermi C, Dubey RN. 2017. Study on out-of-plane behaviour of unreinforced masonry strengthened with welded wire mesh and mortar. *Constr. Build. Mater.* 143:104-120. <https://doi.org/10.1016/j.conbuildmat.2017.03.002>.
14. Kadam SB, Singh Y, Li B. 2014. Strengthening of unreinforced masonry using welded wire mesh and micro-concrete - Behaviour under in-plane action. *Constr. Build. Mater.* 54:247-257. <https://doi.org/10.1016/j.conbuildmat.2013.12.033>.
15. Sistani Nezhad R, Kabir MZ. 2017. Experimental investigation on out-of-plane behavior of GFRP retrofitted masonry panels. *Constr. Build. Mater.* 131:630-640. <https://doi.org/10.1016/j.conbuildmat.2016.11.118>.
16. Gabor A, Bennani A, Jacquelin E, Lebon F. 2006. Modelling approaches of the in-plane shear behaviour of unreinforced and FRP strengthened masonry panels. *Compos. Struct.* 74(3):277-288. <https://doi.org/10.1016/j.compstruct.2005.04.012>.
17. Babaeidarabad S, Arboleda D, Loreto G, Nanni A. 2014. Shear strengthening of un-reinforced concrete masonry walls with fabric-reinforced-cementitious-matrix. *Constr. Build. Mater.* 65:243-253. <https://doi.org/10.1016/j.conbuildmat.2014.04.116>.
18. Carozzi FG, Milani G, Poggi C. 2014. Mechanical properties and numerical modeling of Fabric Reinforced Cementitious Matrix (FRCM) systems for strengthening of masonry structures. *Comp. Struct.* 107:711-725. <https://doi.org/10.1016/j.compstruct.2013.08.026>.
19. Carozzi FG, Poggi C. 2015. Mechanical properties and debonding strength of Fabric Reinforced Cementitious Matrix (FRCM) systems for masonry strengthening. *Compos. B. Eng.* 70:215-230. <https://doi.org/10.1016/j.compositesb.2014.10.056>.
20. Menna C, Asprone D, Durante M, Zinno A, Balsamo A, Prota A. 2015. Structural behaviour of masonry panels strengthened with an innovative hemp fibre composite grid. *Constr. Build. Mater.* 100:111-121. <https://doi.org/10.1016/j.conbuildmat.2015.09.051>.
21. Messali F, Metelli G, Plizzari G. 2017. Experimental results on the retrofitting of hollow brick masonry walls with reinforced high performance mortar coatings. *Constr. Build. Mater.* 141:619-630. <https://doi.org/10.1016/j.conbuildmat.2017.03.112>.
22. Sandoval OJ, Takeuchi C, Carrillo J, Barahona B. 2021. Performance of unreinforced masonry panels strengthened with mortar overlays reinforced with welded wire mesh and transverse connectors. *Constr. Build. Mater.* 267:121054. <https://doi.org/10.1016/j.conbuildmat.2020.121054>.
23. Lucchini S, Facconi L, Minelli F, Plizzari G. 2020. Retrofitting unreinforced masonry by steel fiber reinforced mortar coating: uniaxial and diagonal compression tests. *Mater. Struct.* 53:144. <https://doi.org/10.1617/s11527-020-01574-w>.
24. Facconi L, Fausto M, Vecchio FJ. 2018. Predicting Uniaxial Cyclic Compressive Behavior of Brick Masonry: New Analytical Model. *Journal of Structural Engineering. J. Struct. Eng.* 144(2). [https://doi.org/10.1061/\(ASCE\)ST.1943-541X.0001961](https://doi.org/10.1061/(ASCE)ST.1943-541X.0001961).
25. Corradi M, Agnelli S, Quintaliani C, Speranzini E. 2024. Experimental investigation on a FRCM bio-composite for sustainable retrofitting of masonry buildings. *Compos. Struct.* 329:117753. <https://doi.org/10.1016/j.compstruct.2023.117753>.
26. Xu R, Wang Y, Jiang F, Tang C, Yu J. 2024. Experimental and theoretical studies on the out-of-plane behavior of masonry strengthened with engineered cementitious composite. *Constr. Build. Mater.* 416:135084. <https://doi.org/10.1016/j.conbuildmat.2024.135084>.
27. Codispoti R, Oliveira DV, Olivito RS, Lourenço PB, Fanguero R. 2015. Mechanical performance of natural fiber-reinforced composites for the strengthening of masonry. *Compos. B. Eng.* 77:74-83. <https://doi.org/10.1016/j.compositesb.2015.03.021>.
28. Pachta V, Chatzineofytou K. 2024. Performance of brick masonry prisms retrofitted with fiber reinforced lime-based grouts. *Constr. Build. Mater.* 411:134370. <https://doi.org/10.1016/j.conbuildmat.2023.134370>.
29. Toledo Filho RD, Silva FA, Fairbairn, EMR, Filho JAM. 2009. Durability of compression molded sisal fiber reinforced mortar laminates. *Constr. Build. Mater.* 23(6):2409-2420. <https://doi.org/10.1016/j.conbuildmat.2008.10.012>.
30. Defoirdt N, Biswas S, de Vriese L, Van Acker J, Ahsan Q, Gorbatikh L, Vuure VA, Verpoest I. 2010. Assessment of the tensile properties of coir, bamboo and jute fibre. *Compos. Part A Appl. S.* 41(5):588-595. <https://doi.org/10.1016/j.compositesa.2010.01.005>.
31. Fidelis MEA, Toledo Filho RD, de Andrade Silva F, Mobasher B, Müller S, Mechtcherine V. 2019. Interface characteristics of jute fiber systems in a cementitious matrix. *Cem. Concr. Res.* 116:252-265. <https://doi.org/10.1016/j.cemconres.2018.12.002>.
32. Lima PRL, Santos RG, Ferreira SR, Toledo Filho RD. 2014. Characterization and treatment of sisal fiber residues for cement-based composite application. *Eng. Agrícola.* 34(5):812-825. <https://doi.org/10.1590/S0100-69162014000500002>.
33. Ferreira SR, Silva FA, Lima PRL, Toledo Filho RD. 2017. Effect of hornification on the structure, tensile behavior and fiber matrix bond of sisal, jute and curauá fiber cement based composite systems. *Constr. Build. Mater.* 139:551-561. <https://doi.org/10.1016/j.conbuildmat.2016.10.004>.
34. Ferreira SR, Silva FDA, Lima PRL, Toledo Filho RD. 2015. Effect of fiber treatments on the sisal fiber properties and fiber-matrix bond in cement-based systems. *Constr. Build. Mater.* 101(1):730-740. <https://doi.org/10.1016/j.conbuildmat.2015.10.120>.
35. Jo BW, Chakraborty S, Kim H. 2016. Efficacy of alkali-treated jute as fibre reinforcement in enhancing the mechanical properties of cement mortar. *Mater Struct.* 49:1093-1104. <https://doi.org/10.1617/s11527-015-0560-3>.
36. Silva FA, Filho RDT, Filho JAM, Fairbairn EMR. 2010. Physical and mechanical properties of durable sisal fiber-cement composites. *Constr. Build. Mater.* 24(5):777-785. <https://doi.org/10.1016/j.conbuildmat.2009.10.030>.
37. Ahmad J, Arbili MM, Majdi A, Althoey F, Farouk Deifalla A, Rahmawati C. 2022. Performance of concrete reinforced with jute fibers (natural fibers): A review. *J. Eng. Fibers Fabr.* 17. <https://doi.org/10.1177/15589250221121871>.
38. Majumder A, Stochino F, Frattolillo A, Valdes M, Mancusi G, Martinelli E. 2023. Jute fiber-reinforced mortars: mechanical response and thermal performance. *J. Build. Eng.* 66:105888. <https://doi.org/10.1016/j.job.2023.105888>.
39. Saha S, Mohanty T. 2023. Effects on jute fiber and ferrochrome slag as coarse aggregate on mechanical properties of reinforced concrete. *Mater. Today Proc.* <https://doi.org/10.1016/j.matpr.2023.06.382>.
40. Kesikidou F, Stefanidou M. 2019. Natural fiber-reinforced mortars. *J. Build. Eng.* 25:100786. <https://doi.org/10.1016/j.job.2019.100786>.
41. Toledo Filho RD, Ghavami K, England GL, Scrivener K. 2003. Development of vegetable fibre-mortar composites of improved durability. *Cem. Concr. Compos.* 25(2):185-196. [https://doi.org/10.1016/S0958-9465\(02\)00018-5](https://doi.org/10.1016/S0958-9465(02)00018-5).

42. Bisanda ETN. 2000. The Effect of Alkali Treatment on the Adhesion Characteristics of Sisal Fibres. *Appl. Compos. Mater.* 7:331–339. <https://doi.org/10.1023/A:1026586023129>.
43. FAO. 2023. Jute, kenaf, sisal, abaca, coir and allied fibres Statistical bulletin 2022. Rome.
44. Companhia Nacional de Abastecimento (CONAB). 2023. Análise mensal Juta-Malva 2023. Retrieved from <https://www.conab.gov.br>.
45. Data Bridge Market Research. 2021. Global natural fibre textile market – industry trends and forecast to 2028. *Materials & Packaging, Global*. Retrieved from <https://www.databridgemarketresearch.com/reports/global-natural-fibre-textile-market>.
46. ASTM C1557-20. 2020. Standard test method for tensile strength and young's modulus of fibers.
47. ASTM C618-03. 2017. Standard specification for coal fly ash and raw or calcined natural pozzolan for use in concrete.
48. Lima PRL, Toledo Filho RD. 2008. Use of metakaolin to improve the durability of sisal fiber- cement based composites. *Ambiente Construído*. 8(4):7-19. <https://seer.ufg.br/index.php/ambienteconstruido/article/view/5723>.
49. ABNT NBR 13276. 2016. Mortars applied on walls and ceilings — Determination of the consistence index.
50. ABNT NBR 13278. 2005. Mortars Applied on walls and ceilings - Determination of the specific gravity and the air entrained content in the fresh stage.
51. ABNT NBR 9778. 2009. Hardened mortar and concrete -Determination of water absorption by immersion - Void index and mass specific.
52. Madhavi K, Vinay GN, Renuka Devi MV, Basutkar SM. 2019. Shear behavior of brick masonry strengthened with jute fiber reinforced composite. *Mater. Today Proc.* 46(10):4746–4751. <https://doi.org/10.1016/j.matpr.2020.10.307>.
53. Lee G, Park JH, Pham KVA, Lee CH, Lee K. 2021. Experimental investigation of traditional clay brick and lime mortar intended for restoration of cultural heritage sites. *Appl. Sci.* 11(13):6228. <https://doi.org/10.3390/app11136228>.
54. Arisoy B, Ercan E, Demir A. 2015. Strengthening of brick masonry with PVA fiber reinforced cement stucco. *Constr. Build. Mater.* 79:255-262. <https://doi.org/10.1016/j.conbuildmat.2014.12.093>.
55. ABNT NBR 15270-3. 2005. Ceramic components - Part 3: Structural and non-structural ceramic blocks – Test methods.
56. ASTM E519/E519M – 15. 2022. Standard test method for diagonal tension (shear) in masonry assemblages. ASTM Committee C15 on Manufactured masonry units.
57. RILEM TC-76-LUM. 1994. Diagonal tensile strength tests of small wall specimens, RILEM recommendations for the testing and use of constructions materials, 488-9.
58. Fidelis MEA, de Andrade Silva F, Toledo Filho RD. 2014. The Influence of fiber treatment on the mechanical behavior of jute textile reinforced concrete. *Key Eng. Mater.* 600:469-474. <https://doi.org/10.4028/www.scientific.net/KEM.600.469>.
59. Ferreira SR, Martinelli E, Pepe M, de Andrade Silva F, Toledo Filho RD. 2016. Inverse identification of the bond behavior for jute fibers in cementitious matrix. *Compos. B. Eng.* 95:440–452. <https://doi.org/10.1016/j.compositesb.2016.03.097>.
60. Savastano Júnior H, Agopyan V. 1997. Microstructure X performance of composites reinforced with vegetable fibers. In. São Paulo: Polytechnic School, University of São Paulo.
61. Cottrell JA, Ali M, Tatari A, Martinson DB. 2023. Effects of Fibre Moisture Content on the Mechanical Properties of Jute Reinforced Compressed Earth Composites. *Constr. Build. Mater.* 373:130848. <https://doi.org/10.1016/j.conbuildmat.2023.130848>.
62. Santos DOJ. 2020. Development of lightweight sandwich panels with faces made of cementitious composites reinforced with short sisal fibers and a core made of rice husk bioconcrete, Federal University of Rio de Janeiro, 144p.
63. Daramola OO, Balogun OA, Adediran AA, Saka SO, Oladele IO, Akinlabi ET. 2021. Tensile, flexural, and morphological properties of jute/oil palm pressed fruit fibers reinforced high density polyethylene hybrid composites. *Fibers.* 9(11):71. <https://doi.org/10.3390/fib9110071>.
64. SODOKE FK, TOUBAL L, LAPERRIÈRE L. 2016. Hygrothermal effects on fatigue behavior of quasi-isotropic flax/epoxy composites using principal component analysis. *J. Mater. Sci.* 51(24):10793–10805. <https://doi.org/10.1007/s10853-016-0291-z>.
65. Kumar Verma Y, Kumar Singh A, Paswan MK, Kumar Sonker P. 2023. Importance of functionalized jute fibers in the field of Nano cellulose for the preparation of biodegradable nano composites. *Mater. Today Proc.* 80(1):254-257. <https://doi.org/10.1016/j.matpr.2023.01.031>.
66. Baheti V, Abbasi R, Militky J. 2012. Ball milling of jute fibre wastes to prepare nanocellulose. *World J. Eng.* 9(1):45-50. <https://doi.org/10.1260/1708-5284.9.1.45>.
67. Sinha E, Rout SK. 2009. Influence of fibre-surface treatment of jute fibre and its composite. *Bull. Mater. Sci.* 32:65-67. <https://doi.org/10.1007/s12034-009-0010-3>.
68. Fidelis MEA, Pereira TVC, Gomes ODFM, de Andrade Silva F, Toledo Filho RD. 2013. The effect of fiber morphology on the tensile strength of natural fibers. *J. Mater. Res. Technol.* 2(2):149–157. <https://doi.org/10.1016/j.jmrt.2013.02.003>.
69. Murugan RB, Gayke A, Natarajan C, Haridharan MK, Murali G, Parthiban K. 2018. Influence of Treated Natural Jute Fiber on Flexural Properties of Reinforced Concrete Beams. *Int. J. Eng. Technol.* 7(3.12):148-152. <https://doi.org/10.14419/ijet.v7i3.12.15906>.
70. Santa-Maria H, Duarte G, Garib A. 2004. Experimental investigation of masonry panels externally strengthened with CFRP laminates. 13th World Conference on Earthquake Engineering. 1627-1627.
71. Yu, JH, Park JH. 2020. Investigation of steel fiber-reinforced mortar overlay for strengthening masonry walls by prism tests. *Appl. Science.* 10(18):6395. <https://doi.org/10.3390/app10186395>.
72. Mezrea PE, Ispir M, Balci IA, Bal IE, Ilki A. 2021. Diagonal tensile tests on historical brick masonry wallets strengthened with fabric reinforced cementitious mortar. *Struct.* 33:935-946. <https://doi.org/10.1016/j.istruc.2021.04.076>.
73. Elgwady MA, Lestuzzi P, Badoux Dynamic M. 2002. In-plane behaviour of URM wall upgraded with composites. 3rd International Conference on Composites in Infrastructure. San Francisco, CA, USA.
74. Khaleel S, Madhavi K, Basutkar SM. 2021. Mechanical characteristics of brick masonry using natural fiber composites. *Mater. Today Proc.* 46:4817-4824. <https://doi.org/10.1016/j.matpr.2020.10.319>.
75. Dong Z, Deng M, Dai J, Ping M. 2021. Diagonal compressive behavior of unreinforced masonry walls strengthened with textile reinforced mortar added with short PVA fibers. *Eng. Struct.* 246:113034. <https://doi.org/10.1016/j.engstruct.2021.113034>.